catalysts

MDPI

Article

Synthesis of Hollow Mesoporous TiN Nanostructures as An Efficient Catalyst Support for Methanol Electro-Oxidation

Yoon-Hee Kim, Hyeonkyeong Lee, Dong-Seop Choi, Jiyull Kim, Hyun-Sung Jang, Na-Yeon Kim and Ji-Bong Joo *

Department of Chemical Engineering, Konkuk University, Gwangjin-gu, Seoul 05029, Korea; julia444@konkuk.ac.kr (Y.-H.K.); hyeonk@konkuk.ac.kr (H.L.); cds1105@konkuk.ac.kr (D.-S.C.); jiyull0630@konkuk.ac.kr (J.K.); jhs159@konkuk.ac.kr (H.-S.J.); kny960403@konkuk.ac.kr (N.-Y.K.)
* Correspondence: jbjoo@konkuk.ac.kr; Tel.: +82-2-450-3545

Abstract: The development of efficient catalyst materials that can drive high catalytic performance is challenging. Here, we report a well-defined hollow mesoporous TiN nanostructure for use as Pt catalyst support material for methanol electro-oxidation. The hollow TiN nanostructure was synthesized by the ammonia nitridation of pre-synthesized mother hollow anatase TiO_2, which was prepared by SiO_2 template-assisted sol–gel synthesis followed by chemical etching, acid treatment, and sequential calcination. The variation in the ammonia nitridation temperature allowed the crystalline properties of the samples to be finely tuned. As the ammonia nitrification temperature increased, the crystallinity of the resulting hollow TiN continuously increased, and the corresponding Pt catalysts showed enhanced activity toward methanol electro-oxidation. The hollow TiN-800 sample (H-TiN-800), with a well-developed pure TiN phase, exhibited the highest electrical conductivity and the lowest resistance. The corresponding Pt/H-TiN-800 catalyst exhibited significantly enhanced catalytic activity. In this study, we systemically analyzed the physicochemical characteristics and electrochemical performance of hollow TiN samples and their corresponding Pt catalysts.

Keywords: hollow nanostructure; titanium nitride (TiN); electrocatalyst; ammonia nitrification; methanol electrooxidation; Pt catalyst

Citation: Kim, Y.-H.; Lee, H.; Choi, D.-S.; Kim, J.; Jang, H.-S.; Kim, N.-Y.; Joo, J.-B. Synthesis of Hollow Mesoporous TiN Nanostructures as An Efficient Catalyst Support for Methanol Electro-Oxidation. *Catalysts* **2021**, *11*, 763. https://doi.org/10.3390/catal11070763

Academic Editor: Vignesh Kumaravel

Received: 14 May 2021
Accepted: 21 June 2021
Published: 23 June 2021

1. Introduction

The energy crisis is becoming one of the biggest issues faced by society, directly impacting human life currently and in the near future. Fuel cell technology has great potential as a future power source for a wide variety of energy applications including electric vehicles and mobile electronics [1–6]. Among the different types of fuel cells, direct methanol fuel cells (DMFCs) are possible alternative power sources for portable electronic devices, mobile drones, and robots [7–9]. It is well known that a methanol electro-oxidation occurs in the anode and that an oxygen reaction occurs in the cathode in DMFC systems as follows [10]:

$$\text{Anode: } CH_3OH + H_2O \rightarrow 6H^+ + 6e^- + CO_2$$

$$\text{Cathode: } 3/2O_2 + 6H^+ + 6e^- \rightarrow 3H_2O$$

$$\text{Overall: } CH_3OH + 3/2O_2 \rightarrow 3H_2O + CO_2$$

It is well known that the performance of an electrode catalyst is highly affected by the active metals and support materials used [5,6,11–14]. For Pt-based active metals, Pt or bimetallic Pt-M nanoparticles should be highly dispersed on support materials without any aggregation in order to utilize their large active surface [15–20]. In addition, because

the characteristics of the support materials can have a significant influence on both the activity and stability of the supported Pt catalysts under harsh electrochemical reaction conditions, it is necessary that the support materials have advantageous properties such as high electrical conductivity, inertness under harsh conditions, and favorable morphology for the efficient diffusion of reactants and products [21,22].

In the past decades, extensive studies have been conducted on carbon-supported Pt catalysts for anodic methanol electro-oxidation [23–25]. Conventional carbon materials (e.g., carbon black Vulcan XC-72) are generally used as supports in electrochemistry, and the resulting Pt/C catalysts exhibit excellent performance for anodic methanol electro-oxidation under ambient temperature conditions [26,27]. Although conventional carbons have beneficial features for fabricating Pt/C catalysts that can be used in practical fuel cell systems, several obstacles remain to be overcome, such as resistance to CO poisoning, stability related to carbon corrosion during long-term operation, and limited conductivity for facile electron transfer [6,24,28]. Thus, it is still challenging to find and apply support materials for Pt-based electrocatalysts that have excellent characteristics such as high mechanical stability and outstanding electrical conductivity.

Titanium nitride (TiN) is an extremely hard ceramic material. Because TiN has an intrinsically low friction coefficient, it is often applied as a coating for alloys, steel, carbide, and other materials in order to improve their surface properties. It is also thermally stable and inert in most chemical environments. In addition, it has an extra electron that is not involved in the formation of covalent bonds between Ti and N, which has a significant effect on the conductive characteristics of TiN. Owing to its outstanding characteristics (namely, chemical and thermal stability with high electronic conductivity) TiN has been extensively investigated as an electrode material for supercapacitor or fuel cell applications [29,30]. It is well known that Pt-supported TiN catalysts show not only enhanced CO tolerance but also remarkable stability to electrochemical corrosion during long-term operation for both the anodic methanol oxidation reaction and cathodic oxygen reduction reaction [6,24,28,31]. It has also been reported that TiN-supported Pt catalysts exhibit excellent support stability and that unique interactions between Pt and the TiN support occur, resulting in enhanced catalytic activity for methanol electro-oxidation [32]. Although there have been extensive investigations related to the synthesis and application of TiN as a support material, there are limited studies related to the use of nanostructured TiN materials for catalytic applications. Since TiN nanostructures can provide more opportunities to enhance catalytic activity in various applications, it is still desirable to investigate various nanostructured TiN materials.

It is well known that hollow nanostructures exhibit beneficial characteristics in catalytic reactions and are considered efficient catalyst models that can enhance catalytic performance by improving reaction kinetics [33–35]. Hollow nanostructures with a porous shell layer possess a large surface area per unit mass. The nanoscale shell layer not only provides a short diffusion pathway but also allows reactant molecules to easily access the active site. In addition, once the overall dimension of the hollow nanostructure is in the submicron range, the hollow particles can be easily dispersed in liquid solvent, minimizing the diffusion resistance between the reactant molecules and the surface. These favorable diffusion and dispersion characteristics are beneficial for heterogeneous catalysis. In addition, hollow shell layers with nanoscale dimensions can be easily functionalized. In particular, both the inner and outer surfaces can be selectively functionalized with different active sites, resulting in the ability to induce either confined catalysis or cascade reactions. Hollow TiO_2 nanostructures have been successfully applied as photocatalysts for photocatalytic organic decomposition and hydrogen production [36,37]. Moon et al. also synthesized hollow TiN nanostructures and demonstrated a superior performance in supercapacitor applications compared to a solid TiN counterpart [38]. Based on previous studies and our hypothesis, it is believed that hollow TiN materials with excellent conductivity will be good candidates for conductive scaffolds in electrocatalytic reactions.

In this work, we synthesize a hollow TiN nanostructure that is used as a support material of a Pt-supported catalyst for methanol electro-oxidation. The hollow TiN nanos-

tructure was synthesized by preparing a hollow anatase TiO_2 nanostructure, followed by conversion to a hollow TiN counterpart by ammonia nitridation at different temperatures. As the nitridation temperature increased, the TiN crystallinity of the resulting hollow samples continuously increased. The prepared hollow TiN samples exhibited advantageous characteristics, such as uniform particle dimensions, finely controlled crystallinity, and enhanced electrochemical conductivity. When the Pt nanoparticles were deposited on TiN-800 (prepared by ammonia nitridation at 800 °C), the resulting Pt/H-TiN-800 sample exhibited excellent electrochemical performance for methanol electro-oxidation. In this paper, we discuss the physicochemical characteristics and electrochemical performance of hollow TiN samples and their corresponding Pt catalysts.

2. Results and Discussion

Figure 1 shows a schematic illustration of the procedure for preparing hollow TiN nanostructure samples and Pt/hollow TiN catalysts, as well as corresponding TEM images for each step. To synthesize the hollow TiN nanostructure, pre-synthesized hollow anatase TiO_2 was charged on nitridation using ammonia flow. Hollow anatase TiO_2 was synthesized by a template-assisted sol–gel method, followed by sequential chemical treatments and calcination [36]. Uniform silica particles were synthesized using the well-known Stober method [39]. The monodisperse silica particles were approximately 180 nm in size (Figure 1b). The silica was charged to the TiO_2 coating and the SiO_2@TiO_2 core-shell nanostructure was successfully synthesized by the sol–gel coating of the TiO_2 precursor (Titanium (IV) n-butoxide), as shown in Figure 1c. NaOH treatment was performed to form a hollow nanostructure. Because the dissolution rate of silica is much faster than that of TiO_2 in an aqueous NaOH solution, the silica core was preferentially dissolved, resulting in a hollow TiO_2 nanostructure. As shown in Figure 1d, well-defined hollow TiO_2 spheres were formed after NaOH etching. Because NaOH-treated hollow TiO_2 has many Na^+ ions in its shell matrix, they can be exchanged with H^+ ions by simple acid treatment, as previously reported [36]. A simple acid treatment of the NaOH-etched TiO_2 with a diluted HCl solution was found to convert sodium titanate into protonated titanate, helping not only to preserve the pure titania phase but also to allow for precise control of the TiO_2 crystallinity [36,37]. Thus, hollow anatase TiO_2 can be easily obtained by calcining acid-treated hollow TiO_2 at 800 °C. To synthesize hollow TiN, the hollow anatase TiO_2 was heat-treated under an ammonia environment at different temperatures. Although hollow anatase TiO_2 was treated under ammonia conditions, the structural integrity of the resulting hollow TiN was well maintained, as shown in Figure 1e. After the deposition of colloidal Pt nanoparticles on the surface of the hollow TiN sample, it could be used as an electrocatalyst for methanol electro-oxidation.

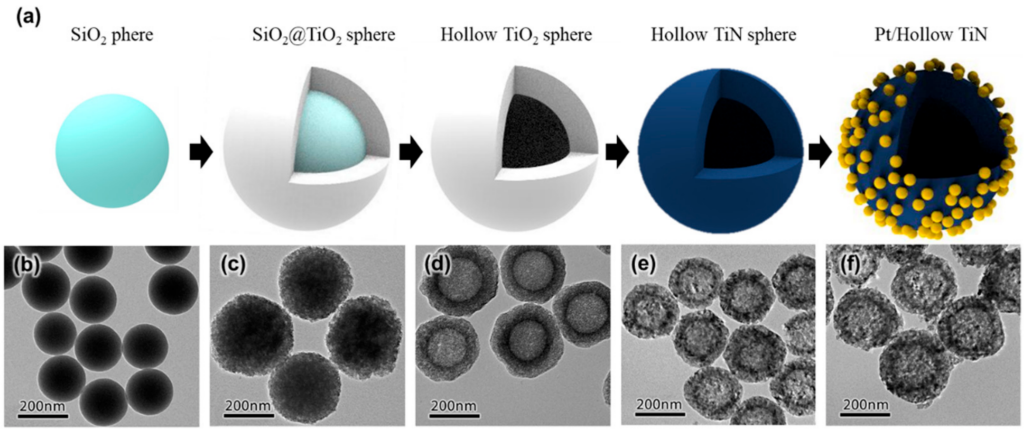

Figure 1. (**a**) Schematic illustration of hollow TiN nanostructures and Pt/hollow TiN catalyst synthesis. Corresponding TEM images of (**b**) SiO_2 sphere; (**c**) SiO_2@TiO_2 sphere; (**d**) hollow TiO_2 sphere; (**e**) hollow TiN-800 sphere; and (**f**) hollow TiN-800 supported Pt catalyst (Pt/H-TiN-800).

The crystalline characteristics of the pre-synthesized hollow TiO_2 and hollow TiN samples were investigated by X-ray diffraction (XRD). As shown in Figure 2, the NaOH-etched H-TiO_2 exhibited amorphous characteristics. It is well known that TiO_2 materials synthesized by sol–gel reactions generally exhibit amorphous characteristics [36,40]. After HCl treatment followed by calcination at 800 °C, the hollow anatase TiO_2 sample (H-anatase TiO_2) showed typical diffraction peaks of the anatase phase at 2θ = 25.4°, 37.8°, 48.1°, 54.0°, 55.1°, and 62.7° that were attributed to the (101), (004), (200), (105), (211), and (204) planes, respectively. When ammonia treatment was carried out at a high temperature, new diffraction peaks appeared. When ammonia nitridation was carried out at 700 °C (H-TIN-700), the sample exhibited mainly anatase diffraction peaks with minor peaks at 2θ = 36.8°, 42.6°, 61.9°, and 74° related to the (111), (200), (220), and (311) planes of TiN, respectively. As the ammonia nitridation temperature increased, the peaks related to the TiN phase intensified and the peaks related to anatase decreased significantly. The XRD pattern of H-TIN-750 comprised a major TiN phase with a minor anatase phase. When an even higher temperature was used during nitridation (800 °C: H-TiN-800), the sample showed sharp peaks related to pure TiN. This indicates that all the anatase crystals were converted to pure TiN by ammonia nitridation at high temperatures. Although there is a chance for the anatase phase to be converted to the rutile phase during ammonia nitridation (as reported by Moon et al.), phase transformation from anatase TiO_2 to the TiN phase mainly occurred in our work. It seems that the phase transformation from anatase TiO_2 to TiN preferentially occurs rather than that from anatase TiO_2 to its rutile counterpart in this work [38]. The average crystalline sizes of the samples were calculated using the Scherrer formula. The average anatase grain sizes were estimated to be approximately 10.7, 9.8, 7.7, and 0 nm for H-anatase TiO_2, H-TiN-700, H-TiN-750, and H-TiN-800, respectively. The TiN grain size exhibited a different trend. The average TiN crystalline sizes were estimated to be approximately 0, 14.2, 15.7 and 16.7 nm for H-anatase TiO_2, H-TiN-700, H-TiN-750, and H-TiN-800, respectively. This indicates that anatase TiO_2 was continuously converted to the TiN phase as the nitridation temperature increased.

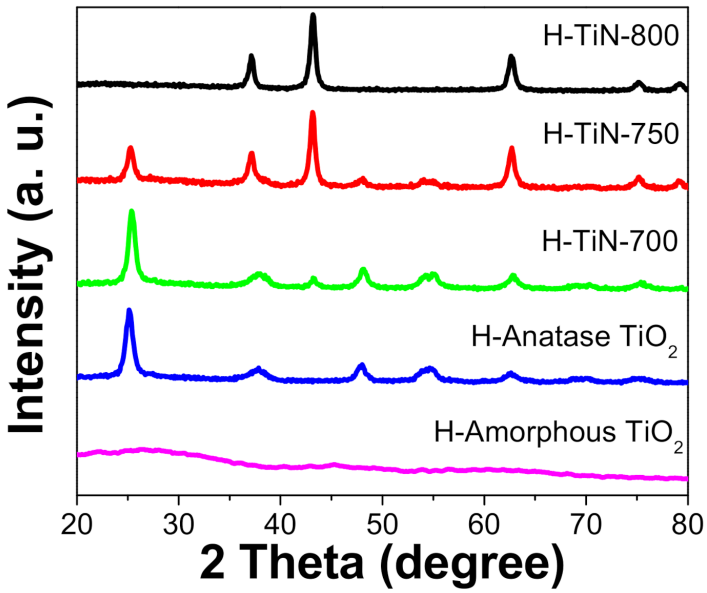

Figure 2. XRD patterns of hollow TiO_2 and TiN samples treated at different temperatures during ammonia nitridation.

We also investigated the textural properties of hollow anatase TiO_2 and hollow TiN samples. As shown in Figure 3, both H-anatase TiO_2 and H-TiN samples exhibited a well-developed hysteresis loop in the range of P/P_0 = 0.4–0.8. This indicates that both samples had well-developed mesoporous structures. As previously reported, mesoporous charac-

teristics should originate from inter-grain mesopores resulting from the crystallization of the amorphous TiO_2 shell to the formation of crystallized grains during calcination [40,41]. Both H-anatase TiO_2 and H-TiN samples showed similar N_2 adsorption values at low relative pressures (P/P_0 = 0–0.2), indicating a similar surface area. The calculated values of the BET surface area for H-anatase TiO_2, H-TiN-700, H-TiN-750, and H-TiN-800 were 66, 64, 70, and 71 m^2/g, respectively. The H-anatase TiO_2 sample exhibited distinct distribution peaks within the mesopore range (1–15 nm) in the BJH pore size distribution, indicating the existence of mesoporosity in the TiO_2 shell layer. After ammonia nitridation, although the TiN samples showed slightly shifted distribution peaks in the mesopore range (1–20 nm), they also exhibited similar mesopores. Based on the N_2 adsorption results, it can be concluded that the textural properties of the samples were not significantly changed through ammonia nitridation.

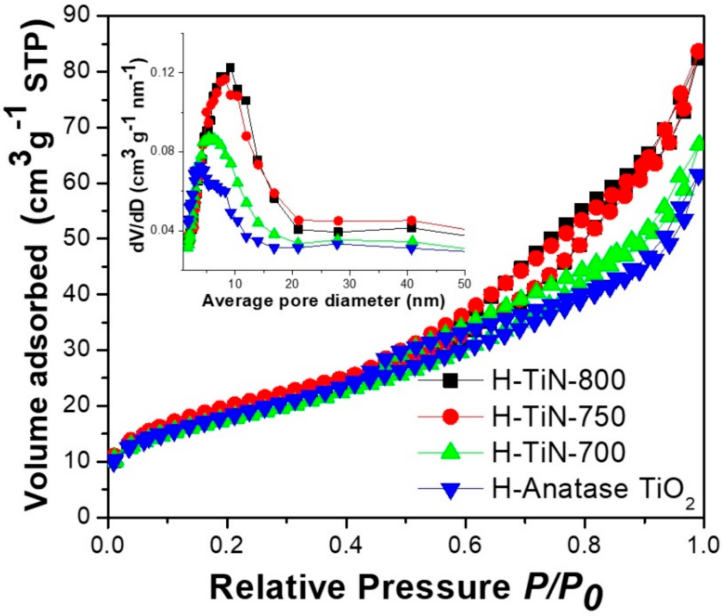

Figure 3. Nitrogen adsorption/desorption isotherms and pore size distributions (inset) of hollow TiO_2 and TiN samples treated at different temperatures during ammonia nitridation.

After the deposition of colloidal Pt nanoparticles on either H-anatase TiO_2 or H-TiN supports, the crystalline properties of the Pt-deposited catalysts were also investigated. As shown in Figure 4, Pt/H-anatase TiO_2 showed diffraction peaks related to its anatase phase, which are identical to the peaks observed in the H-anatase TiO_2 support in Figure 2. In addition, distinct peaks related to fcc Pt were observed at 2θ = 39.7°, 46.2° and 67.4°, attributed to the Pt (111), Pt (200), and Pt (220) planes, respectively. Pt/TiN-700 also exhibited identical diffraction peaks for both anatase TiO_2 and TiN, compared with the mother TiN support and it had distinct peaks related to Pt nanoparticles. The Pt/TiN-750 and Pt/TiN-800 samples also exhibited similar trends. The average crystallite size of the supported Pt particles was estimated using the Scherrer equation based on the Pt (220) diffraction peaks since the Pt (220) peak was isolated from the other peaks [5]. The estimated Pt particle sizes in Pt/H-anatase TiO_2, Pt/H-TiN-700, Pt/H-TiN-750, and Pt/H-TiN-800 were 2.7, 2.7, 2.8, and 2.7 nm, respectively. In addition, the surface areas of Pt were calculated from the crystallite size obtained by the Scherrer equation using the following equation:

$$S = 6000/(d \cdot \rho),$$

where d is the average crystallite size (nm), ρ is the density of Pt (21.4 g/cm^3), and S is the surface area of Pt crystallite (m^2/g_{Pt}). The surface areas of Pt crystallite on Pt/H-anatase TiO_2, Pt/H-TiN-700, Pt/H-TiN-750, and Pt/H-TiN-800 were estimated to be 103, 103,

100, and 103 m^2/g_{Pt}, respectively. Based on the XRD results, we can conclude that the chemical characteristics of the support materials were well maintained even after colloidal Pt deposition. In addition, all the catalysts showed comparable Pt dispersions with similar particle sizes.

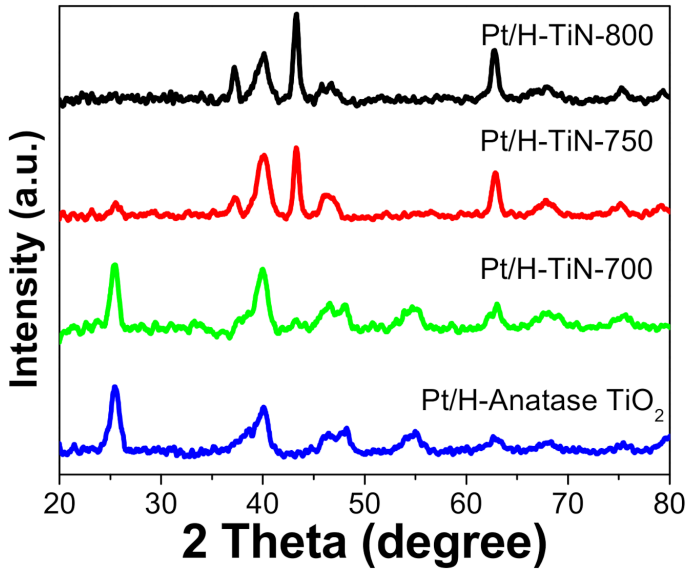

Figure 4. XRD patterns of hollow TiO_2 and hollow TiN supported Pt catalysts.

To investigate the electrochemical characteristics of both the hollow anatase TiO_2 and H-TiN samples, electrochemical measurements were conducted. Figure 5 shows the cyclic voltammograms (CVs) and electrochemical impedance spectroscopy (EIS) Nyquist plots of H-anatase TiO_2, H-TiN-700, H-TiN-750, and H-TiN-800. As shown in Figure 5a, all samples display quasi-rectangular CV patterns without any obvious oxidation/reduction peaks. This indicates that all samples exhibit electric double-layer capacitance in this potential region. The H-TiN-800 sample exhibited the best capacitive properties among the samples. The relative order of the capacitance was as follows: H-anatase $TiO_2 \leq$ H-TiN-700 < H-TiN-750 < H-TiN-800. It should be noted that the electrochemical characteristics of the TiN samples were significantly enhanced as the TiN crystallinity increased. Continuous CV experiments were also carried out using H-TiN-800 and H-anatase TiO_2 in order to evaluate the stability of the support materials. The CV results of H-TiN-800 exhibited negligible variation between the first and hundredth cycles, even though there was a minor change in the anodic scan in the potential range of −0.1–0.8 V (Figure S1, Supporting information). This indicates that the H-TiN-800 sample was sufficiently stable under the harsh electrochemical conditions.

The electrochemical properties were further confirmed using the EIS results, as shown in Figure 5b. The EIS Nyquist plots of all samples exhibited typical semi-circular shapes. It is generally accepted that an EIS Nyquist plot with a small radius indicates a low resistance and good conductance. The smaller arc indicates low charge transfer impedance at the electrode-electrolyte interface. Of the four samples employed as catalyst supports in this work, H-TiN-800 exhibited the smallest arc radius, suggesting that it has the best conductive characteristics. As shown in Figure 4, H-TiN-800 has the highest TiN crystallinity and must have the most conductive TiN framework. Thus, it has the smallest arc among the samples employed. The relative arc size is in the order: H-anatase TiO_2 > H-TiN-700 > H-TiN-750 >H-TiN-800. It indicates that the relative conductivity increases in the order: H-anatase TiO_2 < H-TiN-700 < H-TiN-750 < H-TiN-800. This trend was consistent with the CV measurements. The improved electrochemical performance can be attributed to the intrinsic electronic properties of the TiN samples, such as their low electronic resistance. It is well known that TiN can offer an electronically conducting framework and allow fast

charge transfer, inducing rapid electrochemical redox reactions. Furthermore, the TiN structure displayed better capacitance than its TiO_2 counterpart [38]. In this work, we synthesized hollow anatase TiO_2 and converted it to hollow TiN by ammonia nitridation at different temperatures. As the nitridation temperature increased, the TiN crystallinity of the resulting H-TiN sample was enhanced. Thus, the electrochemical properties of the resulting TiN samples can be significantly improved, which is desirable in electrochemical devices.

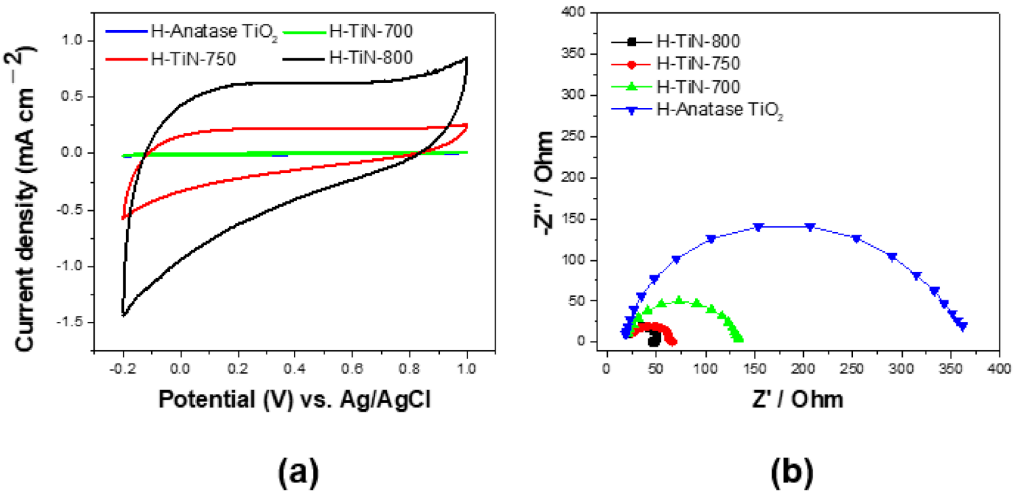

Figure 5. (**a**) CV curves and (**b**) EIS Nyquist plots of hollow TiN samples treated at different nitridation temperatures in 0.5 M H_2SO_4 conditions.

The electrochemical active surface area (ECAS) and electrochemical characteristics of both the Pt/H-anatase-TiO_2 and Pt/H-TiN catalysts were investigated. Figure 6 shows the CV curves of the prepared Pt catalysts in an acidic electrolyte (0.5 M H_2SO_4), which were used to estimate the ECAS using the Coulombic charge for H^+ ion adsorption–desorption. The CV curves of the Pt/H-TiN catalysts showed a typical H^+ ion adsorption/desorption region, a double-layer charging region, a Pt pre-oxidation region, and a Pt reduction region. The peak area for the H^+ ion desorption current was used to estimate the ECAS values, which were calculated from the integrated charge after correction for the contribution of the double-layer charging current using the following equation:

$$S_{ECSA} = \frac{Q_H}{210 \times W_{Pt}},$$

where S_{ECSA}, Q_H, and W_{Pt} are the ECSA value (m^2/g_{Pt}), total charge for H^+ ion desorption (μC), and Pt loading on the electrode (mg/cm^2), respectively. The value 210 is the charge density ($\mu C/cm^2{}_{Pt}$) required to oxidize a monolayer of H^+ ions on the clean Pt surface. The ECSA values for Pt/H-anatase TiO_2, Pt/H-TiN-700, Pt/H-TiN-750, and Pt/H-TiN-800 were 6.7, 16.7, 29.7, and 82.6 m^2/g_{Pt}, respectively.

Similar to the CV results for the support materials, the CV current densities and ECAS values of the corresponding Pt catalysts were improved as the TiN crystallinity was enhanced with increasing nitridation temperature. As shown in Figure 6, the Pt/H-TiN-800 sample showed the largest H^+ ion adsorption–desorption region, resulting in the largest ECAS value. As confirmed by the BET and XRD results (Figures 3 and 4), both surface area values obtained for each support material were similar, and the Pt crystallite sizes of all supported Pt catalysts were similar. This indicates that the Pt dispersion should be almost identical physically since the same amount of Pt is loaded on each support material having a similar surface area by an identical synthetic method. Thus, variations in the CV results of the supported Pt catalysts should be highly influenced by the characteristics of the support materials. As the TiN crystallinity increased, the electrochemical performance of the corresponding Pt catalysts was significantly enhanced,

owing to the advantageous characteristics of the TiN support such as low resistance and high electrical conductivity. Thus, the H-TiN-800 support with the pure TiN phase and highest crystallinity should be the most conductive, resulting in the corresponding Pt/H-TiN-800 exhibiting the most distinct H^+ ion adsorption/desorption current and the most enhanced electrochemical characteristics.

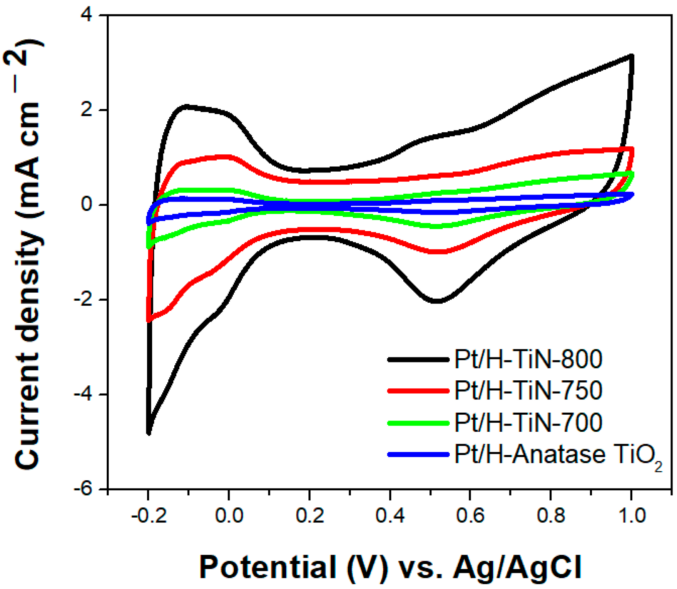

Figure 6. CV curves of hollow TiN supported Pt catalysts at a scan rate of 50 mV/s in 0.5 M H_2SO_4.

To evaluate the electrocatalytic activity of the prepared Pt catalysts, CV was performed in a H_2SO_4 solution in the presence of a methanol solution. Figure 7 shows the CVs of the prepared Pt catalysts in a 0.5 M H_2SO_4 electrolyte containing 2 M CH_3OH. The methanol electro-oxidation current changed negligibly between −0.2 and 0.2 V. The current dramatically increased after 0.2 V, and the maximum peak current was observed at approximately 0.68–0.7 V. After 0.7 V, the current decreased since the number of Pt active sites was reduced owing to the formation of the Pt oxide surface. Above 0.85 V, the current increased again, indicating that methanol oxidation proceeded on the Pt-oxide surface. In the cathodic cycle, the active sites were recovered, resulting in the appearance of a methanol oxidation current peak. We evaluated the catalytic activity of the prepared Pt catalysts by comparing the maximum peak currents during the anodic scan. The relative maximum peak current density was in the order: Pt/H-anatase TiO_2 < Pt/H-TiN-700 < Pt/H-TiN-750 < Pt/H-TiN-800. It should be noted that Pt/H-TiN-800 had the highest current density among the Pt catalysts employed in this study. This indicates that Pt/H-TiN-800 had the highest catalytic activity for methanol electro-oxidation.

It is well known that electrocatalytic activity is significantly influenced by the intrinsic characteristics of either the supported Pt catalysts or support materials [5,6,24,28,31]. Because Pt catalysts supported on different support (containing an identical amount of Pt loaded on the support and with a similar metal dispersion) were used on the working electrode, it can be concluded that the variation in catalytic activity can be explained by the different intrinsic characteristics of the support materials used. As previously mentioned, the higher the TiN crystallinity, the more electrically conductive the support will be [6,28,31,38]. The H-TiN-800 sample exhibited a high crystallinity of the pure TiN structure. This not only facilitated electron transfer but also reduced electrical resistance during electrochemical reactions. Thus, the Pt/H-TiN-800 catalysts can undergo active electrochemical reactions without severe resistance to electron transfer. However, because of the larger electron transfer resistance of Pt/H-anatase TiO_2, due to the semiconducting characteristics of the TiO_2 support, it is believed that slow electron transfer determines the overall reaction rate.

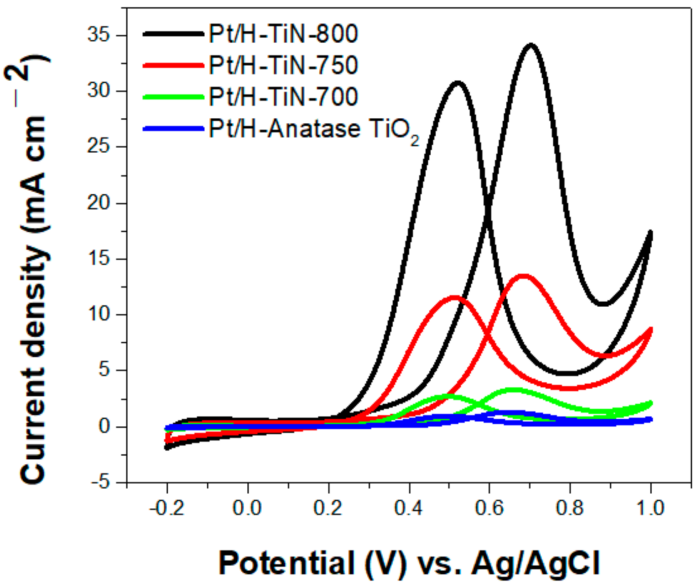

Figure 7. CV curves of hollow TiN-supported Pt catalysts at a scan rate of 50 mV/s in 0.5 M H_2SO_4 containing 2 M CH_3OH.

To investigate how ammonia nitridation at higher temperatures influences the characteristics of the TiN support and the corresponding Pt catalysts, we also prepared hollow TiN nanostructures by ammonia nitridation at 900 °C (H-TiN-900) and synthesized the corresponding Pt catalyst (Pt/H-TiN-900). As shown in Figure S2, H-TiN-900 exhibited a smaller surface area value (35 m^2/g) as well as poorer CV results. This indicates that ammonia nitridation at 900 °C induces a decrease in surface area due to the excessive growth of TiN crystallites, even though it might improve the electrical conductivity. The smaller surface area of H-TiN-900 can induce a lower Pt dispersion in the resulting Pt/H-TiN-900 catalyst. As a result, Pt/H-TiN-900 has a smaller ECAS value (40 m^2/g_{Pt}), resulting in poorer performance than the Pt/H-TiN-800 catalysts. Because ammonia nitridation at 800 °C produces an electrically conductive TiN phase with a large surface, it can be concluded that 800 °C is the optimal temperature.

In addition, the electron that is not involved in the formation of covalent bonds creates electron-abundant environments in TiN. This can be transferred to the supported Pt nanoparticles and cause Pt to exist in a more reduced state. As shown in Figure 8, the Pt 4f XPS peaks of Pt/H-TiN-800 showed more negative values of binding energy (70.98 and 74.21 eV for Pt $4f_{7/2}$ and Pt $4f_{5/2}$, respectively) than those of Pt/H-anatase TiO_2 (71.11 and 74.34 eV for Pt $4f_{7/2}$ and Pt $4f_{5/2}$, respectively). This indicates that Pt/H-TiN-800 has a more active metallic Pt surface than Pt/H-anatase TiO_2. Because methanol electro-oxidation occurs easily on the surface of metallic Pt, Pt/H-TiN-800 exhibits outstanding activity.

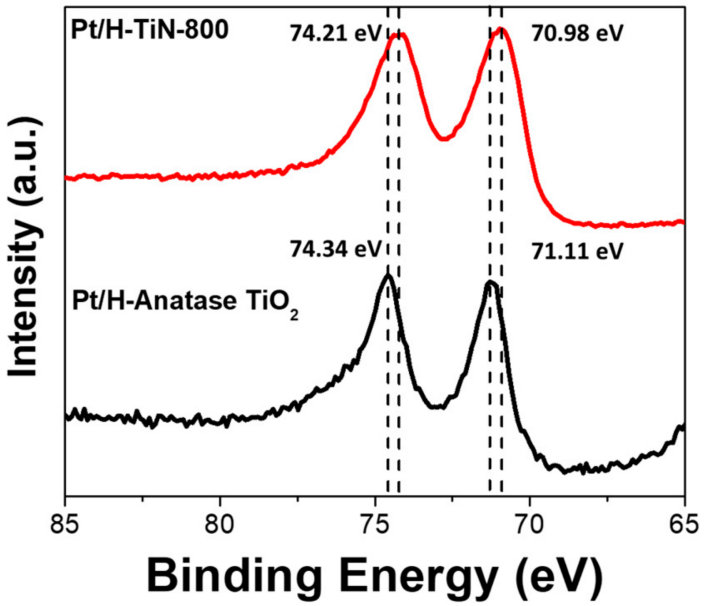

Figure 8. Pt 4f XPS results of Pt/H-Anatase TiO_2 and Pt/H-TiN-800 catalysts.

3. Materials and Methods

3.1. Materials

Ethyl alcohol (C_2H_5OH, 99.9%, anhydrous), methyl alcohol (CH_3OH, 99.9% anhydrous), acetonitrile (ACN, CH_3CN 99.9%, special guaranteed grade), and ammonium hydroxide (NH_4OH, 28%) were obtained from Daejung Chemical Company (Gyeonggi-Do, Korea). Tetraethyl orthosilicate (TEOS, 98%) was purchased from the Samjun Chemical Company (Seoul, Korea). Titanium (IV) n-butoxide (97%, reagent grade), hydroxypropyl cellulose (HPC, MW $\approx$ 80,000), and sodium dodecyl sulfate (SDS, 99%, ACS reagent grade) were obtained from Aldrich Chemical Company (St. Louis, MI, USA). Pt precursor ($H_2PtCl_6 \cdot 6H_2O$) was purchased from Kojima Chemical Company (sayama, Japan). All chemicals were used as received.

3.2. Synthesis

Hollow TiN nanostructures were prepared by converting pre-synthesized anatase hollow particles into their TiN counterparts by ammonia nitridation at different temperatures (700–800 °C). First, hollow anatase TiO_2 particles were synthesized by silica template-assisted sol–gel synthesis followed by sequential base etching, acid treatment, and calcination at 800 °C.

3.2.1. Synthesis of Sacrificial SiO_2 Template

Tetraethyl orthosilicate (1 mL) was mixed with 23 mL of ethanol and 4 mL of deionized water under vigorous stirring. Aqueous ammonia (0.75 mL, 27.5%) was then added and the mixture was stirred at room temperature. After stirring for 3 h, the white precipitate was isolated by centrifugation and washed three times with ethanol. The white precipitate consisted of spherical SiO_2 particles that were used as sacrificial templates in the following synthetic procedures.

3.2.2. Synthesis of Hollow Anatase TiO_2 Shell

The SiO_2 particles were dispersed in a mixture of ethanol (75 mL) and ACN (28 mL). An ethanolic solution of HPC (4 mL, 50 mg/mL) and an ammonia solution (0.8 mL, 27.5%) was then added to the aformentioned mixture. Titanium tert-butoxide (4 mL) was added to a mixture of ethanol (12 mL) and acetonitrile (4 mL). The mixture was stirred for 4 h and washed five times with ethanol and deionized water. The washed

precipitate was comprised of SiO_2@amorphous TiO_2 core-shell particles. The synthesized SiO_2@amorphous TiO_2 core-shells were re-dispersed in an aqueous NaOH solution (25 mL, 0.5 M) and stirred for 24 h for complete etching of the SiO_2 core particles. The precipitate was washed five times with deionized water and ethanol. The isolated precipitate consisted of amorphous TiO_2 hollow particles.

The hollow TiO_2 particles were re-dispersed in deionized water. A diluted HCl solution (0.01 M) was slowly added to the above mixture until the pH of the solution was reduced to approximately 1.5. After stirring for 30 min, the resulting precipitates were isolated by centrifugation, washed with deionized water, and dried under vacuum. The dried samples were calcined at 800 °C for 3 h in air in order to obtain hollow anatase TiO_2 nanostructures.

3.2.3. Synthesis of Hollow TiN Shell

The as-prepared hollow anatase TiO_2 samples were placed in a continuous quartz tubular furnace under N_2 (50 mL/min) and NH_3 (20 mL/min) flow. The temperature was increased by 2.5 °C/min and maintained at the desired temperature (700, 750, or 800 °C) for 10 h. After cooling to ambient temperature, the hollow TiN nanostructure samples were obtained.

3.2.4. Synthesis of Hollow TiN-Supported Pt Catalysts

Hollow TiN-supported Pt catalysts were prepared using the colloidal-immobilization method. Briefly, the desired amount of Pt precursor ($H_2PtCl_6 \cdot 6H_2O$) was dissolved in a mixture of deionized water (90 mL) and methanol (30 mL) under vigorous stirring. Next, SDS (2.956 g) was added to the above solution. After stirring for 10 min, the pre-synthesized hollow TiN samples (100 mg) were well dispersed. Once the TiN was homogeneously dispersed, the mixture was heated to 90 °C and stirred for 1 h. During stirring, the Pt precursor was reduced in order to form colloidal Pt nanoparticles. The solution was then quickly cooled using an ice-water bath while being stirred vigorously. During this process, colloidal Pt nanoparticles were deposited on the surface of the TiN support. The precipitates were isolated by centrifugation and washed seven times with deionized water and ethanol. Finally, hollow TiN-supported Pt catalysts (Pt/H-TiN-X, where X is the ammonia nitridation temperature) were obtained after drying under vacuum. To confirm Pt loading, the amount of Pt in the supported catalysts was estimated by FE-SEM-EDS. The EDS spectra indicated that the Pt loading in the prepared Pt catalysts was approximately 20 wt% (Figure S3).

3.3. Characterization

The particle morphologies were observed by transmission electron microscopy (TEM, JEM-2100, JEOL, Tokyo, Japan). The crystalline properties of the samples were investigated using XRD (D/MAX 2200, Rigaku, Tokyo, Japan). The textural properties were investigated by N_2 adsorption/desorption at 77 K using a N_2 sorption instrument (TriStar II, Micrometrics, Norcross, GA, USA). XPS spectra were recorded on a Thermo K-alpha X-ray photoelectron spectrometer, Waltham, MA, USA).

3.4. Electrochemical Characterization and Methanol Electro-Oxidation

The electrochemical characteristics of the prepared samples were measured using a conventional three-electrode system with an Ag/AgCl electrode and Pt wire as the reference and counter electrodes, respectively. The working electrode was prepared by coating a catalyst ink containing the Pt/H-TiN catalyst and Nafion ionomer on the glass carbon surface. The potential or current was controlled and recorded using a BioLogics SP-150 potentiostat (BioLogic, Seyssinet-Pariset, France). CVs were obtained at a scan rate 50 mV/s in N_2-purged H_2SO_4 solution (0.5 M) from −0.2 to 1.0 V versus the Ag/AgCl electrode. To compare the catalytic activity, CVs were obtained in an N_2-purged H_2SO_4 solution (0.5 M) containing CH_3OH (2 M).

4. Conclusions

We successfully synthesized hollow TiN nanostructures and used them as support materials for Pt catalysts for methanol electro-oxidation. The hollow TiN nanostructures were synthesized using the following sequential steps: (1) synthesis of a sacrificial SiO_2 template; (2) sol–gel coating of TiO_2 on the SiO_2 surface to form a SiO_2@TiO_2 core-shell structure; (3) NaOH etching to remove the template followed by sequential acid treatment and calcination to form H-anatase TiO_2; and (4) ammonia nitridation to convert H-anatase TiO_2 to its H-TiN counterpart. Ammonia nitridation at various temperatures induced different TiN crystalline characteristics. As the nitridation temperature increased, TiN crystallinity was continuously developed, and a pure TiN crystalline structure was obtained at higher temperatures. H-TiN-800 displayed many beneficial characteristics, such as facile electron transfer and low electrical resistance. It also provided an electron-abundant environment and allowed Pt to exist in an active metallic state. The resulting Pt/H-TiN-800 exhibited significantly enhanced catalytic activity toward methanol electro-oxidation. We believe that the hollow TiN materials developed in this study can provide a good solution for developing highly active catalyst materials for various electrochemical applications.

Supplementary Materials: The following are available online at https://www.mdpi.com/article/10.3390/catal11070763/s1. Figure S1: Continuous CV experiment results of H-TiN-800 and H-Anatase TiO_2 before and after 100 cycling between −0.1 V and 0.8V in 0.5 M H_2SO_4 conditions. Figure S2: (a) Nitrogen adsorption/desorption isotherms of H-TiN-800 and H-TiN-900. CV results of Pt/H-TiN-800 and Pt/H-TiN-900 (b) in 0.5 M H_2SO_4 and (c) in 0.5 M H_2SO_4 containing 2 M CH_3OH. Figure S3: FE-SEM images, element mapping results and EDS spectra with element composition of (a–e) Pt/H-Anatase TiO_2, and (f–j) Pt/H-TiN-800.

Author Contributions: Investigation, writing—original draft preparation, Y.-H.K.; investigation, methodology, resources, H.L.; methodology, resources, D.-S.C.; resources, J.K.; visualization, H.-S.J.; resources, N.-Y.K.; conceptualization, writing—review and editing, supervision, J.-B.J. All authors have read and agreed to the published version of the manuscript.

Funding: This work was supported by a National Research Foundation of Korea (NRF) grant funded by the Korean government (MSIT) (No. NRF-2021R1A2C1012242). This research was also supported by KETEP/MOTIE of the Republic of Korea. (Grant no. 20194010201790).

Acknowledgments: This work was supported by a National Research Foundation of Korea (NRF) grant funded by the Korean government (MSIT) (No. NRF-2021R1A2C1012242). This research was also supported by KETEP/MOTIE of the Republic of Korea. (Grant no. 20194010201790).

Conflicts of Interest: The authors declare no conflict of interest.

References

1. Joo, J.B.; Kim, P.; Kim, W.; Kim, Y.; Yi, J. Effect of the preparation conditions of carbon-supported Pt catalyst on PEMFC performance. *J. Appl. Electrochem.* **2009**, *39*, 135–140. [CrossRef]
2. Gasteiger, H.A.; Kocha, S.S.; Sompalli, B.; Wagner, F.T. Activity benchmarks and requirements for Pt, Pt-alloy, and non-Pt oxygen reduction catalysts for PEMFCs. *Appl. Catal. B Environ.* **2005**, *56*, 9–35. [CrossRef]
3. Rastler, D. Challenges for fuel cells as stationary power resource in the evolving energy enterprise. *J. Power Sour.* **2000**, *86*, 34–39. [CrossRef]
4. Bernay, C.; Marchand, M.; Cassir, M. Prospects of different fuel cell technologies for vehicle applications. *J. Power Sour.* **2002**, *108*, 139–152. [CrossRef]
5. Joo, J.B.; Kim, N.D.; Yun, H.J.; Kim, P.; Yi, J. Preparation of highly crystalline graphitic nanocarbon for the electro-oxidation of methanol. *Nano Res.* **2011**, *4*, 92–102. [CrossRef]
6. Higgins, D.C.; Choi, J.-Y.; Wu, J.; Lopez, A.; Chen, Z. Titanium nitride–carbon nanotube core–shell composites as effective electrocatalyst supports for low temperature fuel cells. *J. Mater. Chem.* **2012**, *22*, 3727–3732. [CrossRef]
7. Kamarudin, S.K.; Achmad, F.; Daud, W.R.W. Overview on the application of direct methanol fuel cell (DMFC) for portable electronic devices. *Int. J. Hydrogen Energy* **2009**, *34*, 6902–6916. [CrossRef]
8. Joh, H.-I.; Ha, T.J.; Hwang, S.Y.; Kim, J.-H.; Chae, S.-H.; Cho, J.H.; Prabhuram, J.; Kim, S.-K.; Lim, T.-H.; Cho, B.-K.; et al. A direct methanol fuel cell system to power a humanoid robot. *J. Power Sour.* **2010**, *195*, 293–298. [CrossRef]
9. Rashidi, R.; Dincer, I.; Naterer, G.F.; Berg, P. Performance evaluation of direct methanol fuel cells for portable applications. *J. Power Sour.* **2009**, *187*, 509–516. [CrossRef]

10. Gong, L.; Yang, Z.; Li, K.; Xing, W.; Liu, C.; Ge, J. Recent development of methanol electrooxidation catalysts for direct methanol fuel cell. *J. Energy Chem.* **2018**, *27*, 1618–1628. [CrossRef]
11. Joo, J.B.; Kim, Y.J.; Kim, W.; Kim, P.; Yi, J. Simple synthesis of graphitic porous carbon by hydrothermal method for use as a catalyst support in methanol electro-oxidation. *Catal. Commun.* **2008**, *10*, 267–271. [CrossRef]
12. Joo, J.B.; Kim, Y.J.; Kim, W.; Kim, N.D.; Kim, P.; Kim, Y.; Yi, J. Methanol-tolerant PdPt/C alloy catalyst for oxygen electro-reduction reaction. *Korean J. Chem. Eng.* **2008**, *25*, 770–774. [CrossRef]
13. Joo, J.B.; Kim, Y.J.; Kim, W.; Kim, P.; Yi, J. Preparation and Characterization of a PtSn Nanocatalyst for Use in Ethanol Electro-Oxidation. *J. Nanosci. Nanotechnol.* **2008**, *8*, 5130–5134. [CrossRef] [PubMed]
14. Sohn, Y.; Joo, J.B.; Kim, P. Chemically dealloyed Pt–Au–Cu ternary electrocatalysts with enhanced stability in electrochemical oxygen reduction. *Res. Chem. Intermed.* **2018**, *44*, 3697–3712. [CrossRef]
15. Luo, L.; Xu, D.; Li, L.; Li, X. Impact of dehydrogenation on the methanol oxidation reaction occurring on carbon nanotubes supported Pt catalyst with low Pt loading. *Int. J. Hydrogen Energy* **2021**. [CrossRef]
16. Dang, D.; Wang, X.; Yang, X.; Wu, C. Photodeposition and hydrogenation activity of Pt nanosites on the TiN support: Photo-assisted metal-support synergy. *Mol. Catal.* **2020**, *497*, 111206. [CrossRef]
17. Bock, C.; Paquet, C.; Couillard, M.; Botton, G.A.; MacDougall, B.R. Size-Selected Synthesis of PtRu Nano-Catalysts: Reaction and Size Control Mechanism. *J. Am. Chem. Soc.* **2004**, *126*, 8028–8037. [CrossRef] [PubMed]
18. Wu, J.; Xu, M.; Lei, S.; Jin, C. High electrocatalytic activity and stability of PtAg supported on rutile TiO2 for methanol oxidation. *Int. J. Hydrogen Energy* **2020**, *45*, 12815–12821. [CrossRef]
19. Peng, K.; Bhuvanendran, N.; Ravichandran, S.; Zhang, W.; Ma, Q.; Xing, L.; Xu, Q.; Khotseng, L.; Su, H. Carbon supported PtPdCr ternary alloy nanoparticles with enhanced electrocatalytic activity and durability for methanol oxidation reaction. *Int. J. Hydrogen Energy* **2020**, *45*, 22752–22760. [CrossRef]
20. Quintero-Ruiz, J.; Ruiz-Rosas, R.; Quílez-Bermejo, J.; Salinas-Torres, D.; Cazorla-Amorós, D.; Morallón, E. Preparation of Pt/CNT Thin-Film Electrodes by Electrochemical Potential Pulse Deposition for Methanol Oxidation. *C* **2021**, *7*, 32.
21. Xie, F.; Tian, Z.; Meng, H.; Shen, P.K. Increasing the three-phase boundary by a novel three-dimensional electrode. *J. Power Sour.* **2005**, *141*, 211–215. [CrossRef]
22. Yuan, D.; Xu, C.; Liu, Y.; Tan, S.; Wang, X.; Wei, Z.; Shen, P.K. Synthesis of coin-like hollow carbon and performance as Pd catalyst support for methanol electrooxidation. *Electrochem. Commun.* **2007**, *9*, 2473–2478. [CrossRef]
23. Kim, P.; Kim, H.; Joo, J.B.; Kim, W.; Song, I.K.; Yi, J. Preparation and application of nanoporous carbon templated by silica particle for use as a catalyst support for direct methanol fuel cell. *J. Power Sour.* **2005**, *145*, 139–146. [CrossRef]
24. Lee, J.-M.; Han, S.-B.; Song, Y.-J.; Kim, J.-Y.; Roh, B.; Hwang, I.; Choi, W.; Park, K.-W. Methanol electrooxidation of Pt catalyst on titanium nitride nanostructured support. *Appl. Catal. A Gen.* **2010**, *375*, 149–155. [CrossRef]
25. Xiao, Y.; Zhan, G.; Fu, Z.; Pan, Z.; Xiao, C.; Wu, S.; Chen, C.; Hu, G.; Wei, Z. Robust non-carbon titanium nitride nanotubes supported Pt catalyst with enhanced catalytic activity and durability for methanol oxidation reaction. *Electrochim. Acta* **2014**, *141*, 279–285. [CrossRef]
26. Kim, P.; Joo, J.B.; Kim, W.; Kim, J.; Song, I.K.; Yi, J. NaBH4-assisted ethylene glycol reduction for preparation of carbon-supported Pt catalyst for methanol electro-oxidation. *J. Power Sour.* **2006**, *160*, 987–990. [CrossRef]
27. Kim, P.; Joo, J.B.; Kim, W.; Kim, J.; Song, I.K.; Yi, J. Preparation of highly dispersed Pt catalyst using sodium alkoxide as a reducing agent and its application to the methanol electro-oxidation. *J. Mol. Catal. A Chem.* **2007**, *263*, 15–19. [CrossRef]
28. Musthafa, O.T.M.; Sampath, S. High performance platinized titanium nitride catalyst for methanoloxidation. *Chem. Commun.* **2008**, 67–69. [CrossRef] [PubMed]
29. Alhussain, H.; Mise, T.; Matsuo, Y.; Kiyono, H.; Nishikiori, K.; Akashi, T. Influence of ammonia gas exposure on microstructure of nanocrystalline titanium nitride powder synthesized from titanium dioxide. *J. Ceram. Soc. Jpn.* **2019**, *127*, 824–829. [CrossRef]
30. Burke, M.; Blake, A.; Povey, I.M.; Schmidt, M.; Petkov, N.; Carolan, P.; Quinn, A.J. Low sheet resistance titanium nitride films by low-temperature plasma-enhanced atomic layer deposition using design of experiments methodology. *J. Vac. Sci. Technol. A* **2014**, *32*, 031506. [CrossRef]
31. Ottakam Thotiyl, M.M.; Ravikumar, T.; Sampath, S. Platinum particles supported on titanium nitride: An efficient electrode material for the oxidation of methanol in alkaline media. *J. Mater. Chem.* **2010**, *20*, 10643–10651. [CrossRef]
32. Avasarala, B.; Murray, T.; Li, W.; Haldar, P. Titanium nitride nanoparticles based electrocatalysts for proton exchange membrane fuel cells. *J. Mater. Chem.* **2009**, *19*, 1803–1805. [CrossRef]
33. Joo, J.B.; Dahl, M.; Li, N.; Zaera, F.; Yin, Y. Tailored synthesis of mesoporous TiO2 hollow nanostructures for catalytic applications. *Energy Environ. Sci.* **2013**, *6*, 2082–2092. [CrossRef]
34. Joo, J.B.; Zhang, Q.; Dahl, M.; Zaera, F.; Yin, Y. Synthesis, crystallinity control, and photocatalysis of nanostructured titanium dioxide shells. *J. Mater. Res.* **2012**, *28*, 362–368. [CrossRef]
35. Zhang, Q.; Lee, I.; Joo, J.B.; Zaera, F.; Yin, Y. Core–Shell Nanostructured Catalysts. *Acc. Chem. Res.* **2013**, *46*, 1816–1824. [CrossRef]
36. Joo, J.B.; Lee, I.; Dahl, M.; Moon, G.D.; Zaera, F.; Yin, Y. Controllable Synthesis of Mesoporous TiO2 Hollow Shells: Toward an Efficient Photocatalyst. *Adv. Funct. Mater.* **2013**, *23*, 4246–4254. [CrossRef]
37. Joo, J.B.; Liu, H.; Lee, Y.J.; Dahl, M.; Yu, H.; Zaera, F.; Yin, Y. Tailored synthesis of C@TiO2 yolk–shell nanostructures for highly efficient photocatalysis. *Catal. Today* **2016**, *264*, 261–269. [CrossRef]

38. Moon, G.D.; Joo, J.B.; Dahl, M.; Jung, H.; Yin, Y. Nitridation and Layered Assembly of Hollow TiO2 Shells for Electrochemical Energy Storage. *Adv. Funct. Mater.* **2014**, *24*, 848–856. [CrossRef]
39. Stöber, W.; Fink, A.; Bohn, E. Controlled growth of monodisperse silica spheres in the micron size range. *J. Colloid Interface Sci.* **1968**, *26*, 62–69. [CrossRef]
40. Joo, J.B.; Zhang, Q.; Lee, I.; Dahl, M.; Zaera, F.; Yin, Y. Mesoporous Anatase Titania Hollow Nanostructures though Silica-Protected Calcination. *Adv. Funct. Mater.* **2012**, *22*, 166–174. [CrossRef]
41. Lee, H.; Jang, H.S.; Kim, N.Y.; Joo, J.B. Cu-doped TiO2 hollow nanostructures for the enhanced photocatalysis under visible light conditions. *J. Ind. Eng. Chem.* **2021**, *99*, 352–363. [CrossRef]